PAPER

Check for updates

A systematic study of high resolution multielemental quantitative bioimaging of animal tissue using LA-ICP-TOFMS

Stanislav Strekopytov, [ID] Kharmen Billimoria [ID] and Heidi Goenaga-Infante [ID] *

Methodology for quantitative bioimaging of essential metals including Mg, Mn, Fe, Cu and Zn in tissue cryosections based on the use of high-resolution laser ablation coupled with inductively coupled plasma time-of-flight mass spectrometry (LA-ICP-TOFMS) has been systematically developed and characterized for the first time. Cryosectioned gelatin standards spiked with all the elements of interest were used for calibration. Analysis under 'no gas' conditions showed satisfactory selectivity and 3-fold improved limits of detection for Mn, Fe and Cu when compared with those when using 2.4 ml min^{-1} H$_2$ in the collision/reaction cell of the ICP-TOFMS instrument. Absolute single-pixel limits of detection at 3 μm spatial resolution were in the range of 4–9 femtograms for Mn, Cu and Zn and approximately 40 femtograms for Mg and Fe. Gelatin standards spiked with acidified single-element solutions and with solutions prepared from metal salts were shown to have similar elemental homogeneity. The impact of variable thickness of cryosectioned gelatin on the signal intensity was studied and the linearity of response was established for thicknesses between 10 and 30 μm. The developed method was used for the quantification of essential metals in kidney sections of rats dosed with bis-choline tetrathiomolybdate (TTM) to regulate Cu levels in relation with Wilson's disease as well as in kidney sections of control animals. To achieve this, the developed methodology was extended to also include Mo and detailed distribution of Mo/Cu ratios at cellular to subcellular resolution was obtained, showing fine correlation between these elements in the medulla regions of the kidney.

Introduction

Metals in the organism may be essential or beneficial as well as non-essential, harmful, or toxic. The role of each metal is governed by bioinorganic chemistry of the organism or a particular cell type.[1] Metal dysregulation is implicated in the pathology of a range of medical conditions including neurodegenerative disorders such as Alzheimer's disease (AD)[2] and metabolic disorders such as Wilson's disease (WD).[3] In cancer, metals play a role in cancer development, for example, in cancer metastasis and also treatments *via* metal-containing drugs.[4,5] Additionally, metal ions released from metallic implants in the body may be transported and accumulated in organs causing undesirable phenomena.[6] Therefore, visualizing metals distribution in organs and at cellular levels is critical for understanding the role metals play in the body and how their behaviour might correlate to wider physiological functions.

To better understand how metals function and to discriminate between healthy and diseased tissues as well as to compare data over time and between populations, it is imperative to determine both localization and concentration of metals at

LGC Limited, National Measurement Laboratory (NML), Queens Road, Teddington, Middlesex TW11 0LY, UK. E-mail: heidi.goenaga-infante@lgcgroup.com

a cellular to sub-cellular resolution. Laser ablation inductively coupled plasma mass spectrometry (LA-ICP-MS) is the most advanced technique for obtaining spatially resolved information and quantification of metals and many non-metals in thin sections of tissue given its excellent limit of detections (LOD) which are in the range of μg kg^{-1} to mg kg^{-1} and fit-for-purpose spatial resolution (μm to <1 μm range). Quantification of elements in animal tissue sections using LA-ICP-MS has associated remaining challenges, of which the heterogeneity of biological samples and the lack of suitable reference materials are significant. Factors such as ablation properties, transport-related phenomena, ionization in the ICP source, signal drift over analysis time and matrix effects need to be addressed for correct quantification.[7] The possibility to correct for the variability of these factors by using internal standards – either present in the tissue section such as ^{13}C or somehow deposited onto the section or the specimen slide is very limited. Despite many approaches proposed so far, no truly universal calibration and quantification protocol exists for the spatially resolved quantification of metals in biological tissues.[8,9]

One of the main considerations for LA-ICP-MS bioimaging is the maximum imaging speed at which individual pixels of the elemental map are fully resolved. The imaging speed is determined by the highest laser repetition rate available, stability of

the laser energy, speed of the sample stage movement, washout time within the ablation chamber and the sample transfer line as well as the speed of the mass-spectrometric detection.[10] An ability to completely ablate the full thickness of the specimen without sampling the specimen substrate such as soda–lime glass is another consideration and is addressed by either using higher laser wavelength (typically 266 nm)[11] or by carefully controlling laser energy.[12] Development of laser ablation systems in the last few years addressed the imaging speed by providing improved stage control and fast-washout sample transfer solutions.[13] Commercially available laser ablation systems[14,15] using low-dispersion (ultrafast) ablation cell geometries are now capable of pulse-resolved imaging at repetition rates of 100 Hz and above.[16]

At the same time, scanning mass analysers used by the most common ICP-MS instruments introduce restrictions to the number of isotopes that can be detected quasi-simultaneously from sections of a transient ion beam corresponding to individual laser shots. This limitation was a driving force in developing and improving the ICP-MS instrumentation employing time-of-flight (TOF) analysers (ICP-TOFMS), which acquires the entire mass range at short integration times.[17–19] ICP-TOFMS is well-suited for the analysis of short transient events, such as those generated by single-pulse-resolved laser ablation.[20] Although the single-isotope sensitivity for commercially available TOFMS instruments is lower than that obtainable with single-m/z monitoring on quadrupole mass spectrometers (QMS), TOFMS surpasses sequential ICP-MS instruments in total ion sensitivity, which is critical for multielemental analysis.[21] Moreover, modern ICP-TOFMS instruments can record the entire elemental mass range signals at 500 Hz or higher. To achieve artefact-free imaging, triggered acquisition can be employed to enable real-time, spot-resolved multielemental analysis synchronized with the arrival of the aerosol plume of a single laser shot to the ICP-TOFMS.[22] The developments in the ICP-TOFMS provide a solid analytical platform for all areas of solid-state analysis and, in particular, for bioimaging where fast multielemental detection is a paramount.[10,18,23–30]

Quantification strategies for silicate materials in LA-ICP-MS typically include external calibration using one or more certified reference materials (CRMs) with a silicate glass matrix and with the intensity corrected by the intensity of an internal standard (IS). The IS is typically one of the major components of the sample and it may be determined by an independent technique. Using this traditional approach in other areas of solid-state analysis including bioimaging presents a serious challenge since no matrix CRMs are currently available. This is certainly true for most bioimaging applications such as imaging of animal tissue sections and single cells. Chemical elements present in animal tissue at high levels and homogenously distributed (*e.g.*, C, N, O) are not necessarily suitable for LA-ICP-MS analysis and/or for quantification by an independent non-destructive technique and, so, their potential use as IS is limited.

Several materials have been used as calibration standards in LA-ICP-MS bioimaging: inkjet-printed paper,[31] commercially available powdered CRMs with animal tissue matrix,[23,24,32]

spiked agarose film,[33] spiked homogenised tissue,[34] and spiked gelatin.[35] Of those, the closest matrix-matching was likely achieved by using homogenised tissue and gelatin-based preparations. Both materials can be spiked with the elements of interest at different concentration levels, providing multi-point calibration curves, and can be frozen and sliced to the same thickness as the material to be imaged, to provide direct comparison.[35–38]

Over the past few years, calibration with spiked gelatin presented as either cryosections[39–42] or droplets, deposited manually,[43,44] in microarrays[45] or using a microspotter[27,28] or a bioprinter,[30] has largely replaced matrix-matched calibration with spiked homogenised tissue in LA-ICP-MS bioimaging. Despite the wide use of gelatin standards, quantification using gelatin cryosections has not yet been studied systematically and applied to single-shot high-resolution imaging. The limits of this quantification strategy, such as the effect of sample heterogeneity at a single-pixel level and the possibility of using different section thickness for the standard and the sample, have not been discussed in detail so far.

This work describes a systematic approach towards spatial multi-element quantification of several essential metals including Mg, Cu, Zn, Mn and Fe in biological tissue using high resolution LA-ICP-TOFMS and calibration with multi-element spiked cryosectioned gelatin standards. The optimal LA-ICP-TOFMS conditions for achieving a compromise between sensitivity and selectivity were investigated. The effect of the spiking solution (*e.g.*, with pH-neutral salts or HNO_3-based solutions) on the elemental homogeneity of the produced standards was studied. The impact of thickness of cryosectioned gelatin on the signal intensity was studied at thicknesses between 10 and 30 μm and the fit-for-purpose linearity of response was established. Finally, the developed methodology was applied to the quantitative imaging of Mg, Mn, Fe, Cu Zn and Mo in kidney samples of the Sprague Dawley rat following bis-choline tetrathiomolybdate treatment to regulate Cu levels in relation to Wilson's disease.

Experimental

Instrumentation

For all experiments, an imageBIO266 laser ablation system (266 nm, Elemental Scientific Lasers, USA) in combination with a low-dispersion ablation cell in a TwoVol3 ablation chamber was coupled using a 0.8 mm ID PEEK tubing and a Dual Concentric Injector (DCI) to an ICP-TOFMS instrument (icpTOF2R, Tofwerk AG, Switzerland). The tubing length between the laser ablation system and the DCI was kept to a minimum (<15 cm). LA was carried out in a helium atmosphere (99.99% purity, BOC Ltd, UK) and a stream of argon gas (99.99%, BOC Ltd, UK) served as the carrier gas.

The laser ablation settings and ICP-TOFMS settings were optimized daily to achieve high intensities for $^{59}Co^+$, $^{115}In^+$, and $^{238}U^+$ while keeping the oxide level (based on $^{232}Th^{16}O^+/^{232}Th^+$) below 1% and the laser-induced elemental fractionation (based on $^{232}Th^+/^{238}U^+$) at 1 ± 0.2. An in-house prepared gelatin-based

This journal is © The Royal Society of Chemistry 2023

J. Anal. At. Spectrom., 2023, **38**, 704–715 | **705**

material spiked with a range of elements of interest was used for the optimisation of laser ablation and ICP-TOFMS parameters.

The stages of the ablation cell, the laser and the TOFMS data acquisition were triggered using a laser ablation workflow of TofPilot (Tofwerk AG, Switzerland) software.

Preparation of gelatin calibration standards

Calibration standards were prepared from 10% (w/w) aqueous solution of gelatin (gelatin from porcine skin, gel strength $\sim$300 g Bloom, Type A, Sigma-Aldrich®, USA). Gelatin and the appropriate amount of water were weighed in plastic moulds and gravimetrically spiked with a solution of Mg, Mn, Fe, Cu and Zn in 0.5 M HNO_3, prepared from commercial single-element stock solutions of 10 000 mg kg^{-1} (Mg) or 1000 mg kg^{-1} (Mn, Fe, Cu and Zn) (ROMIL Ltd, UK). The final HNO_3 concentration in gelatin solutions did not exceed 0.02 M. Standards prepared for LA-ICP-TOFMS quantification of Mg, Mn, Fe, Cu, Zn and Mo in rat kidney tissue were also spiked with Mo from gravimetric dilutions from a stock solution containing 1000 mg kg^{-1} Mo (ROMIL Ltd, UK). Unspiked gelatin solutions were used for preparing blank samples. The gelatin standards were heated to 60 °C and mixed manually. A 200 μL aliquot of each standard was deposited onto pre-cooled specimen chucks and sectioned to a thickness of 30 μm using low-profile disposable 819 blades in a Leica CM 1850 cryostat (Leica Biosystems, Germany) set to a temperature of –17 °C. Gelatin sections were mounted onto SuperFrost™ (Thermo Fisher Scientific, USA) microscope slides, air-dried at 4 °C and equilibrated at room temperature prior to analysis.

To study the influence of the spike matrix solution on the heterogeneity and overall performance of the gelatin standards, another set of calibration standards was prepared by adding pH-neutral aqueous spikes prepared using $MgCl_2$ (99.9% ultra dry), $MnCl_2 \cdot 4H_2O$ (99.99%), $FeCl_2$ (99.99%), $CuCl_2 \cdot 2H_2O$ (99.999%) and $ZnCl_2 \cdot xH_2O$ (99.99%) (Alfa Aesar™, Thermo Fisher Scientific, USA). Elemental concentrations in pH-neutral solutions used for gelatin spiking were determined by ICP-TOFMS with a solution sample introduction interface. The instrument was calibrated using four calibration standards prepared from a multielemental aqueous CRM (SM68 Standard 1, VHG Labs, LGC Standards, USA).

Confirmation of the elemental concentrations in the prepared gelatin standards was performed as described elsewhere.[46,47]

Samples

Tissue sections were obtained during an animal study described in detail elsewhere.[46] All animal procedures were performed in accordance with the Guidelines for Care and Use of Laboratory Animals of the Commission of Health and Provincial Department of Agriculture and Rural Affair of Jiangsu Province, China and approved by the Animal Ethics Committee of Crown Bioscience Inc. (Taicang, China). Sprague Dawley rats were given bis-choline tetrathiomolybdate (TTM) orally at three dosage levels: 0 mg per kg per day (control group), 15 mg per kg per day (low-dosage group) and 60 mg per kg per day (high-

dosage group). Kidney tissue from one animal in the control group and one from the high-dosage group were chosen for this study. Tissue was flash-frozen in liquid nitrogen and stored at – 80 °C before being cryosectioned at 4 μm thickness. Tissue sections were mounted onto SuperFrost™ (Thermo Fisher Scientific, USA) microscope slides, air-dried at 4 °C and equilibrated at room temperature prior to analysis.

Pulse-resolved multielemental imaging

Typical LA and ICP operating conditions are provided in Table 1. Laser parameters and ablation patterns were set up using ActiveView2 software (Elemental Scientific Lasers, USA). For all experiments, a circular laser beam was focused onto the sample surface. The data acquisition was triggered for every ablation position. To generate consecutive line scans in single-pulse mode, a laser repetition rate of 100 Hz and a sample moving speed of 300 μm s^{-1} were applied, so that positions of successive LA craters were edge-to-edge without overlapping areas. Consecutive lines were ablated in the same direction and spaced 3 μm apart. Complete ablation of the sample was visually confirmed during the analysis. Integrated TOFMS spectra were acquired at 105.53 Hz, which corresponds to the sum-ion spectrum from 206 TOF extractions per data point (block period 9.476 ms). The entire elemental image was acquired as a single continuous Hierarchical Data Format (HDF) file. Gas blank signals were acquired as separate files.

Data processing

Data processing was performed using the data analysis package "Tofware" (version 3.2.0, Tofwerk AG, Switzerland) running in

Table 1 Laser ablation and ICP-MS parameters used in this study

Laser ablation parameters	
Laser fluence	6 J cm^{-2}
Laser spot diameter	3 μm
Laser repetition rate	100 Hz
Laser scan speed	300 μm s^{-1}
Ablation gas flow 1 (He)	0.45 L min^{-1}
Ablation gas flow 2 (He)	0.55 L min^{-1}

ICP-TOFMS parameters	
Carrier gas flow	0.85–0.87 L min^{-1}
Auxiliary gas flow	0.8 L min^{-1}
Cooling gas flow	14 L min^{-1}
RF power	1550 W
Collision/reaction cell (CRC) gas	No gas mode: unpressurized cell Hydrogen mode: 2.4 ml min^{-1} H_2
Notch filter	$^{40}Ar^+$, $^{40}Ar_2^+$
$^{232}Th^+/^{238}U^+$	0.85–1.1
ThO^+/Th^+	<1%
Monitored isotopes	^{24}Mg, ^{25}Mg, ^{26}Mg, ^{55}Mn, ^{56}Fe, ^{57}Fe, ^{63}Cu, ^{65}Cu, ^{64}Zn, ^{66}Zn, ^{68}Zn, ^{95}Mo, ^{98}Mo

the Igor Pro (Wavemetrics, USA) environment. Tofware was used to model and subtract the baseline intensities that elevate the total signal on each m/z channel. Following mass calibration, baseline subtraction, and peak integration of isotopes from every TOFMS spectrum, the integrated signal time traces for all m/z channels were exported as comma-separated values (CSV) files using a TwImage programme (Tofwerk AG, Switzerland). Those m/z channels that had overlapping signals of interfering ions (^{55}Mn, ^{56}Fe, ^{57}Fe, ^{65}Cu) were processed by peak fitting, the rest of the channels by peak integration.[48]

Results and discussion

Selectivity and limits of detection

Despite numerous advantages of ICP-MS, spectral interferences greatly affect the selectivity of the ICP-MS detection of many elements. Spectral overlaps, typically singly or doubly charged atomic and molecular ions, depend on the sample composition and the conditions of the plasma. Quadrupole-based ICP-MS instruments are generally not capable of mass separation of these spectral interferences. The mass resolving power (R_m) of the icpTOF2R is in the range of 5000–6000 (reported as $m/\Delta m$, where Δm is the width of the mass peak at full-width half-maximum; FWHM) and is sufficient to resolve many doubly charged atomic and some molecular interferences. As the TOF mass analyzer measures all ion signals within the measurable m/z range, both the identification of interferences and deconvolution of overlapping mass-spectral peaks are possible. For example, Hendriks et al.[21] showed how peak deconvolution increases R_m effectively about 2-fold and so can isolate the signals of $^{31}P^+$ and $^{68}Zn^+$ from background species ($^{15}N^{16}O^+$, $^{14}N^{16}OH^+$, and $^{40}Ar^{14}N^{14}N^+$, respectively).

However, R_m of the icpTOF2R may not be sufficient when abundant molecular ions need to be separated from the isotopes of interest. Another approach to resolve spectral interferences is to use ion–molecule reactions (using a reaction gas such as H_2) or kinetic energy discrimination (using He as a collision gas) in a multipole ion guide. Burger et al.[49] investigated the impact of using H_2 or He as reaction and/or collision gases in the LA-ICP-TOFMS to target ^{40}Ca and ^{80}Se and improved LODs by orders of magnitude.

In the current work, we have investigated the effect of using H_2 in the collision/reaction cell (CRC) on the selectivity and sensitivity of the simultaneous detection of Mg, Mn, Fe, Cu and Zn. The H_2 flow rate (2.4 ml min^{-1}) was selected at the level at which $^{40}Ar^+$ did not need to be removed from the ion beam by the radiofrequency (RF) quadrupole notch filter. We compared the performance of the fast multielemental LA-ICP-TOFMS imaging under the conditions optimal for their selective determination (hydrogen mode) with that under the conditions optimized for the best overall sensitivity (no gas in the CRC).

The detection of the most abundant isotope of iron (^{56}Fe) by ICP-MS is known to be affected by the $^{40}Ar^{16}O^+$ interference. The effect of H_2 in the CRC on the selectivity of ^{56}Fe detection by LA-ICP-TOFMS was investigated. Fig. 1 shows that $^{57}Fe/^{56}Fe$ values obtained by LA-ICP-TOFMS at 100 Hz repetition rate for five Fe concentration levels (45–400 mg kg^{-1}) with no gas and with 2.4
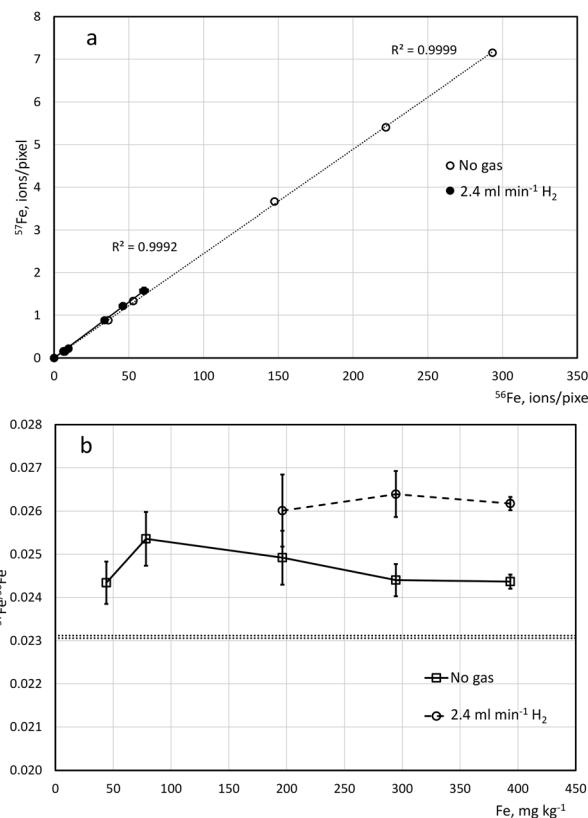

Fig. 1 Relationship between the intensities of ^{57}Fe and ^{56}Fe (a) and the ratio of $^{57}Fe/^{56}Fe$ (b) as detected by LA-ICP-TOFMS, under no-gas conditions in the CRC and using H_2 at 2.4 ml min^{-1}, in gelatin-based standards spiked with Fe at five concentration levels (milligrams per kilogram of dry gelatin). Isotope ratios were only calculated for intensities of ^{57}Fe above 1 count per pixel. Ablation was conducted at 3 μm spot size at 100 Hz laser repetition rate, isotope ratios calculated after subtracting the blank signal. Errors bars represent standard deviation (1sd) between four individual gelatin sections. The natural range of $^{57}Fe/^{56}Fe$ is within the dot lines.

ml min^{-1} H_2 in the CRC are near the range of natural $^{57}Fe/^{56}Fe$ values (0.02306–0.02312).[50] The deviation of the isotope ratios from the natural value (6% and 13% for unpressurized cell and cell pressurized with H_2, respectively) is likely to be explained by the mass bias towards the heavier isotope, known for the ICP-TOFMS instruments.[51,52] The data obtained in this study show that the mass-resolving power of icpTOF2R in combination with peak deconvolution is sufficient for selective low-signal detection of ^{56}Fe. While pressurizing CRC with H_2 has benefits in enabling detection of ^{40}Ca, ^{39}K, and ^{80}Se, it was found to lead to lower single-pixel LOD as the signal suppression due to

Table 2 Single-pixel LOD of the elements in gelatin standards sectioned at 30 μm thickness for 3 μm spot size at 100 Hz repetition rate in LA-ICP-TOFMS

LOD, mg kg^{-1}	^{24}Mg	^{55}Mn	^{56}Fe	^{63}Cu	^{64}Zn
Unpressurized cell	59	3.2	27	10	15
2.4 ml min^{-1} H_2	123	9.2	77	33	17

collision/reaction gas led to poorer counting statistics (Table 2). These results suggest that unless there is a need to include elements affected by the notch filter (e.g., Ca and K) it is more beneficial to conduct multielemental LA-ICP-TOFMS bioimaging under unpressurized conditions (no gas in the CRC), especially when using an instrument with higher mass resolution such as icpTOF2R.

Single-pixel LODs for Mg, Mn, Fe, Cu and Zn (Table 2) have been determined based on the analyte signal obtained by laser ablation of unspiked gelatin. Typically, data for 8500–10 500 pixels were collected for each of the 3–4 individual gelatin sections. The same number of replicates applied for the standards used for the calibration curve.

The compound Poisson distribution that describes the low-count TOFMS signals[53] is dependent on an empirical detector response curve, and thus cannot be simply calculated. This potentially affects the correct determination of LOD for LA-ICP-TOFMS imaging, especially at higher laser repetition rates. However, since most pixels obtained from 30 μm unspiked gelatin sections at 100 Hz were giving non-zero signal (higher than 1 count per pixel), the so-called "IUPAC approximation"[54] is deemed to be satisfactory[24] for the purposes of calculating LOD:

$$\text{Single-pixel LOD} = (3.29\sigma_B + 2.71)/\text{sensitivity},$$

where LOD is the minimum detectable value and σ_B is the standard deviation of the single-pixel measurement of an unspiked gelatin sample.

Influence of the spiking solution on the homogeneity of the gelatin standards

Preparing calibration standards for quantitative LA-ICP-MS bioimaging that would be stable, reproducible and homogenous is a challenging task that has been approached by researchers in a number of ways. Commercially obtained gelatin typically contain very low concentrations of many elements of interest, can be further purified if needed and may be handled in more creative ways than homogenised tissue and so it is often a matrix of choice. As the integrity of gelatin can be compromised by low pH caused by spiking with commercial element stock solution, typically in nitric or hydrochloric acid matrix, spikes prepared from metal salts and/or buffering of the gelatin solution have been proposed.[55] In this study, the homogeneity of the standards prepared with addition of HNO_3-based spikes and with the addition of spikes prepared from nitrate salts without acidification was compared. In chemical imaging, the homogeneity of the sample can be described by the value of single-pixel standard deviation of the analyte signal intensity, assuming the noise produced by heterogeneity is larger than the noise produced by the process of measurement. Therefore, the comparison was conducted based on the values of the between-pixel relative standard deviation (RSD) at two different levels of spiking for Mg and Zn, and at three different level for Mn and Cu (Fig. 2).

To eliminate the effect of spurious pixels (caused by e.g., a dust particle or a bubble in gelatin) on the single-pixel
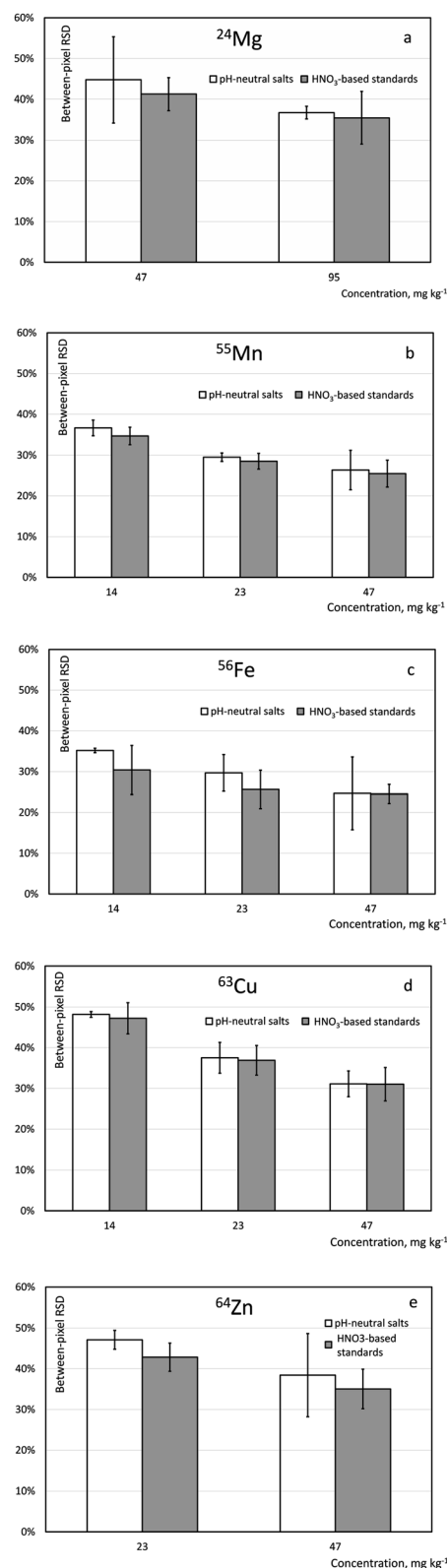

Fig. 2 Single-pixel relative standard deviation (RSD) of the LA-ICP-TOFMS imaging signal for ^{24}Mg, ^{55}Mn, ^{56}Fe, ^{63}Cu and ^{64}Zn (a–e) in gelatin standards spiked at different levels (14–95 milligrams per kilogram of dry gelatin) with pH-neutral salt and HNO_3-based standard solutions, after removal of outliers. Error bars correspond to 1sd between the average responses obtained from three separate cryosections.

708 | J. Anal. At. Spectrom., 2023, **38**, 704–715

This journal is © The Royal Society of Chemistry 2023

standard deviation value the datasets were first checked for outliers. Outliers were defined as the values outside of the $\bar{x} \pm 3\sigma$, where $\bar{x}$ is the arithmetic mean and σ is the standard deviation of the single-pixel measurement. Although both the sample mean and the standard deviation are sensitive to outliers, for large number of points (*ca.* 10 000) and a bell-shaped distribution observed for the data from spiked samples, this approach seems to be justified. The number of outliers found to be 0.3% of the total number of pixels and therefore considered negligible. No difference was observed in the number of outliers between the acid-solution spiked and pH-neutral solution spiked standards. Average intensities for every isotope of interest in each analysed section and single-pixel standard deviations were re-calculated after removing outliers.

Single-pixel standard deviations for the two spiking solutions are shown in Fig. 2. Using a statistical F-test, the standards containing 23 mg kg^{-1} Mn, Fe, Cu and Zn and 47 mg kg^{-1} Mg and prepared from acid-solution spiked and pH-neutral solution spiked standards were compared. No statistical difference was observed for single-pixel standard deviation of analyte signal Mn and Cu, while single-pixel standard deviation for Mg, Fe and Zn was statistically smaller in the acid-solution spiked standard ($\alpha = 0.05$). Therefore, addition to gelatin of an acid-solution matrix spike is deemed to be fit-for-purpose and all the subsequent method development has been conducted using spiking with solutions prepared from HNO$_3$-based single-element stock solutions.

Thickness of gelatin cryosections

The increase in sample load (from increasing sample thickness) may potentially change the plasma and/or transport conditions and thus the amount of analyte ionized in the plasma.[9,56,57] Confirmation of the linearity between the analyte signal intensity and the thickness of cryosections is needed when tissue samples are analysed against calibration based on gelatin cryosections. This is because the matrix of the tissue cryosections differs from those of gelatin standards. To the authors' knowledge, this type of information is still missing for modern low-dispersion LA interfaces.

In the current work, the laser fluence and the repetition rate were kept constant so that gelatin sections are completely ablated but the underlying glass slide is not ablated. The absence of glass ablation was confirmed by monitoring ^{140}Ce, which was found to be abundant in the glass slide coating. Therefore, it is assumed that the particle size distribution of the ablated material remains reasonably invariant.[56]

Excellent linearity of response ($r^2 = 0.998$–0.999) was found for all the elements studied (Mg, Mn, Fe, Cu and Zn) for five different gelatin thicknesses (10, 14, 20, 25 and 30 μm; Fig. 3). It can be thus concluded that sample load does not seem to have a significant effect on the signal intensity of the elements of interest, when low-dispersion LA setup is used and high repetition rate (100 Hz). Previous work focussed on the ^{13}C response with a view of using this isotope as an internal standard in bioimaging.[56,57] Unfortunately, the limitations that most TOF
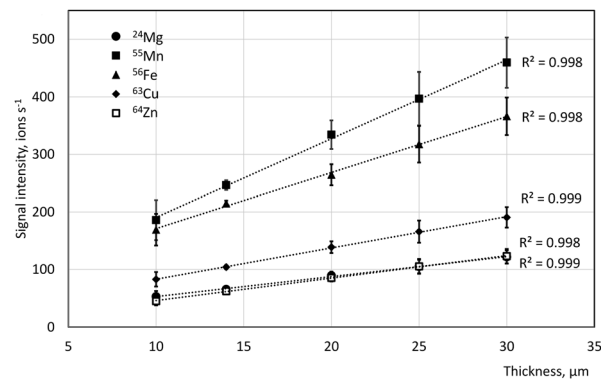

Fig. 3 ^{24}Mg, ^{55}Mn, ^{56}Fe, ^{63}Cu, and ^{64}Zn signal intensity as a function of gelatin cryosection thickness. Concentration of spikes is approximately 670 mg kg^{-1} of dry gelatin for Mg and 330 mg kg^{-1} of dry gelatin for Mn, Fe, Cu and Zn. Error bars correspond to 1sd between signals from individual sections ($n = 4$).

detectors in their standard configuration have in the low-mass range of the mass spectrum makes this impossible or impractical for LA-ICP-TOFMS imaging. The observed linearity of response suggested the use of gelatin cryosections of a single thickness as feasible calibrants for tissue samples sectioned at a range of thicknesses. Thicker sections were found to be more practical for calibration as they require less spike to be added to gelatin to achieve the same amount of analyte per pixel. A gelatin section thickness of 30 μm was selected as optimal for further work.

Application of the developed calibration strategy to quantification of Mg, Mn, Fe, Cu, Zn and Mo in kidney samples of the Sprague Dawley rat following bis-choline tetrathiomolybdate treatment

Elevated copper levels are the cause of diseases, such as Wilson disease (WD)[3] and cancer.[4] One of the most important therapeutic interventions of WD is de-coppering therapy, where tetrathiomolybdate (TTM) is proposed as a copper-sequestering drug.[58] The proposed therapeutic use of molybdenum-based drugs poses a potential risk for accumulation through chronic administration of therapeutic doses of this element. A previous study[46] using LA-ICP-TOFMS to investigate the effect of daily dosing of a molybdenum compound, bis-choline tetrathiomolybdate (TTM) for three months in Sprague Dawley rats as conducted at the resolution of 20 μm, with a view of collecting whole-organ information. Accumulation of Mo in the organs was found to affect the distribution of Cu, due to the chelation effect. The methodology for high resolution (3 μm) multi-elemental quantitative imaging developed in the current work was extended to include Mo originating from the drug and applied to obtain quantitative information on the spatial distribution of both endogenous elements (Mg, Mn, Fe, Cu and Zn) and Mo with focus on the relationship between Cu and Mo at cellular and subcellular levels.

Molybdenum was not included in the systematic method development initially as methodology was intended for multi-element imaging of essential elements in tissue and this
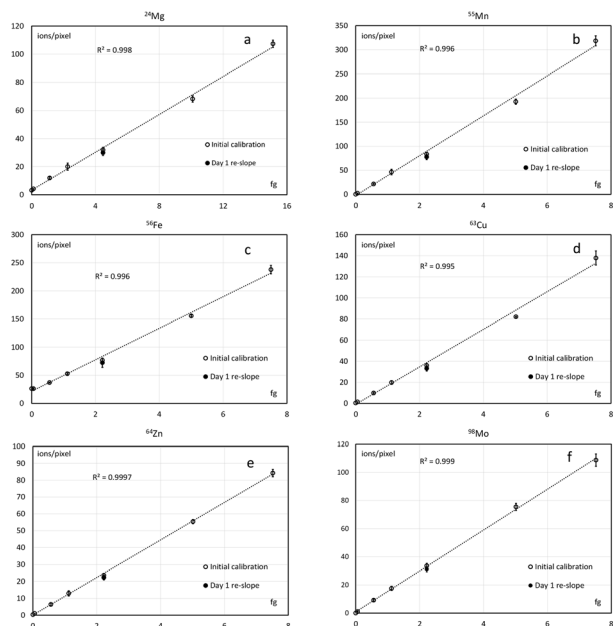
This journal is © The Royal Society of Chemistry 2023

J. Anal. At. Spectrom., 2023, **38**, 704–715 | **709**

Fig. 4 Calibration curves for quantitative LA-ICP-TOFMS imaging of Mg, Mn, Fe, Co, Zn and Mo (a–f) in tissue samples at 3 μm spot size. Error bars correspond to 1sd between individual cryosections ($n = 3$, 30 μm thickness) of spiked gelatin.

Fig. 5 Distributions of Cu (a and b) and Mo (c and d) in rat kidney taken from a control animal (a and c) and from a rat given 60 mg per kg per day TTM (b and d), imaged at pixel size 18 × 20 μm. Colour scale is in fg per pixel. Black rectangle approximately indicated the area used for high-resolution imaging (3 × 3 μm) in the consecutive section (see Fig. 6).

element is typically below the LOD of LA-ICP-MS methodology, even at lower resolution, in natural animal tissue. However, for the purpose of investigating the effect of Mo supplementation on the de-coppering of tissue, the high resolution (3 μm) multielemental quantitative imaging method developed in the current work was extended to also include Mo. For this purpose, LA-ICP-TOFMS monitoring of ^{95}Mo and ^{98}Mo in tissue from Mo-treated animals suggested the lack of matrix-induced interferences, confirming isotopic selectivity.

Quantification was conducted by calibrating the instrument using unspiked gelatin as a blank and six gelatin standards spiked with 4–500 mg kg^{-1} (dry gelatin mass) Mg and 2–250 mg kg^{-1} (dry gelatin mass) Mn, Fe, Cu, Zn and Mo (Fig. 4). Three sections at each level of spiking were analysed and ca. 15 000 pixels collected in each section. Limits of detection (Table 3) have been calculated as described above. Once the calibration curve was established, the organ section could be analysed on the next day(s) and the calibration slope was adjusted by analysing three sections of a single spiking level immediately before and after the analysis of the sample(s). The stability of the slope within 10% of the initial value was confirmed in a separate experiment over at least two weeks of imaging.
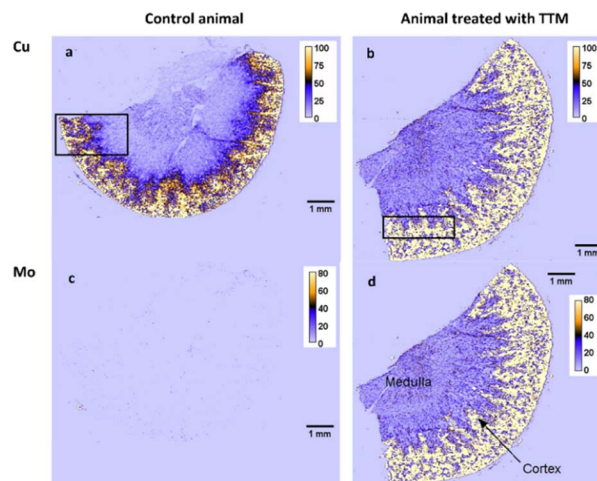
Calibration curve slope expressed in absolute amount of analyte (e.g., femtograms) can be directly used to calculate the amount of corresponding analyte in each individual pixel of the tissue section. When comparing tissues of different thicknesses, analyses performed at different pixel sizes or other reasons require expression in mass fraction (mg kg^{-1}), the conversion can be performed using known or assumed densities of gelatin and tissues samples at the time of sectioning. When the linearity range of the sectioning protocol is established, like in this study, the thicknesses of gelatin and tissues sections may be different. The typical water content in rat tissues is ca. 75%,[59] much lower than in gelatin standards (90%); therefore, it can be argued that the dry thickness of tissue cryosectioned at 4 μm setting is not too dissimilar from the dry thickness of gelatin cryosectioned at 10 μm and, therefore, within the range of LA-ICP-TOFMS linear response established in this study.
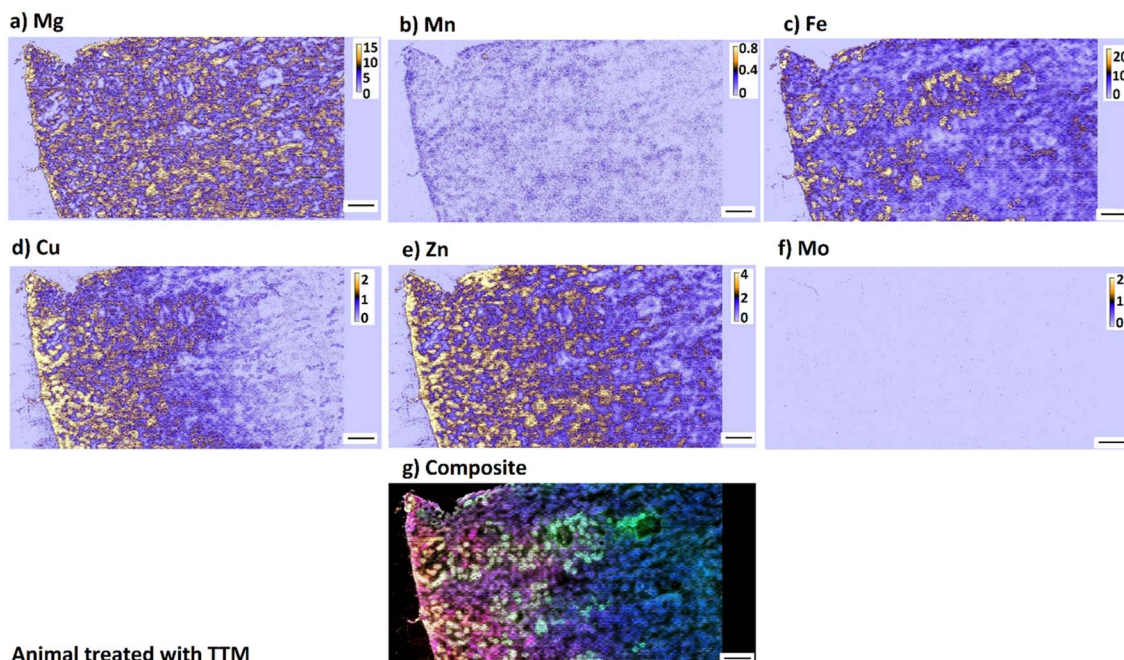
High resolution images reveal a high level of detail which is not accessible when imaging of the whole organ at low resolution (Fig. 5) is performed and thus provide information on the relationship between Mo and Co as well as between endogenous elements (e.g., Cu and Fe, or Cu and Zn) at cellular level. The medulla region of the kidney, which accumulates metals at higher levels (Fig. 6), was chosen for high-resolution imaging in this work.

Table 3 Single-pixel LODs for 3 μm spot size LA-ICP-TOFMS in rat kidney sections at 100 Hz

Isotope	^{24}Mg	^{55}Mn	^{56}Fe	^{63}Cu	^{64}Zn	^{98}Mo
Absolute LOD (fg)	1.7	0.14	1.52	0.28	0.33	0.25
LOD (mg kg^{-1}), 4 μm-thick kidney section	44.7	3.8	40.2	7.3	8.8	6.6

710 | J. Anal. At. Spectrom., 2023, 38, 704–715

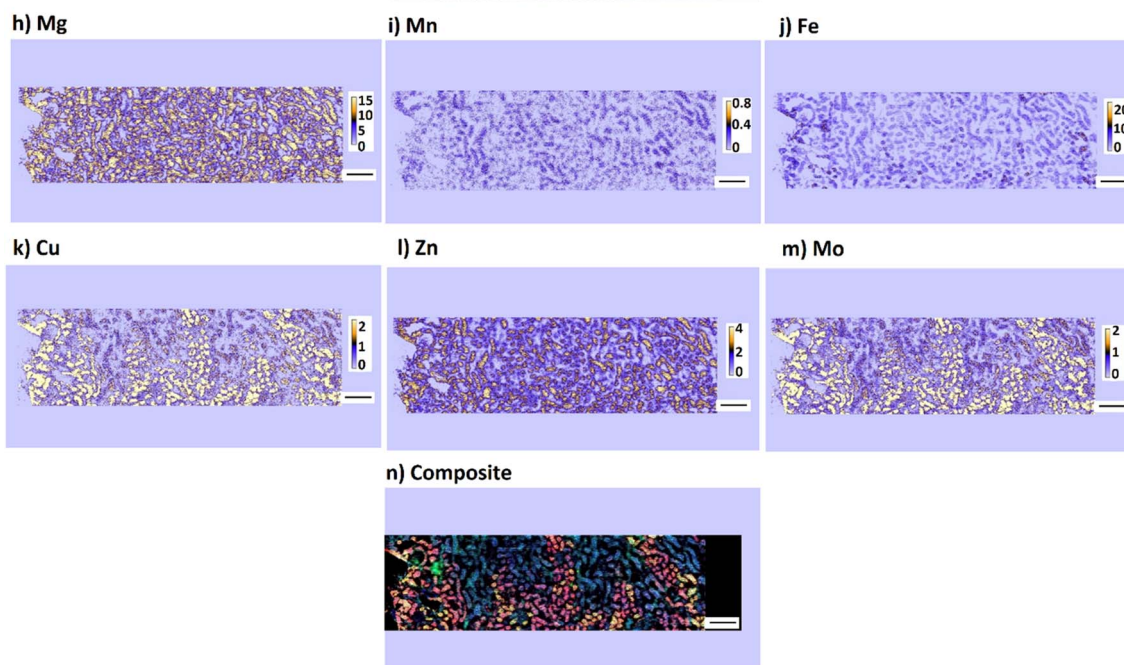This journal is © The Royal Society of Chemistry 2023

Fig. 6 Distribution of Mg, Mn, Fe, Cu, Zn and Mo (a–f, h–m), and a composite image (g, n) (red = Cu, green = Fe, blue = Mg) in rat kidney taken from a control animal (a–g) and from a rat given 60 mg per kg per day TTM (h–n) imaged at 3 μm resolution. The area imaged is approximately indicated in the whole-organ image in Fig. 5. Colour scale is in fg per pixel. Scale bar corresponds to 200 μm. The isotopes measured are ^{24}Mg, ^{55}Mn, ^{56}Fe, ^{63}Cu, ^{64}Zn and ^{98}Mo.

Results from high-resolution imaging confirmed that, in animals treated with TTM, enrichment in Mo correlates with the enrichment in Cu. This is probably related to the mechanism of de-coppering action of TTM which involves a formation of a ternary complex with Cu and blood albumin that is then excreted with urine.[60] However, the distribution of Mo/Cu ratio in individual pixels was found to depend greatly on the resolution chosen (Fig. 7). While lower resolution images give the impression of the near-normal distribution of the Mo/Cu ratio, high-resolution images reveal a more complex pattern that suggests bimodal distribution. The histograms of Mo/Cu distribution at 3 μm spot size calculated separately for high-Mo concentrations (>64 mg Mo kg^{-1}) and for low-Mo concentrations (LOD < Mo < 64 mg kg^{-1}) show two distinctly different

This journal is © The Royal Society of Chemistry 2023
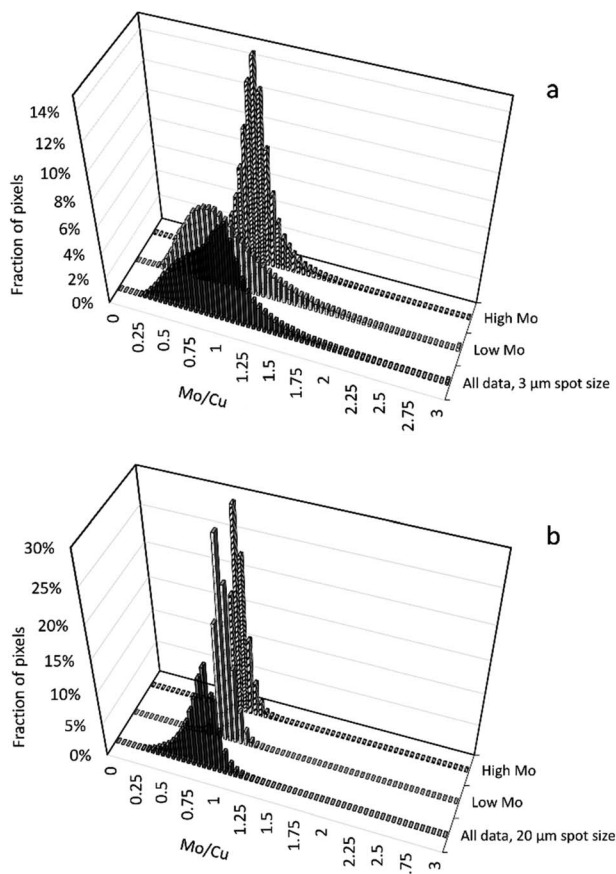
J. Anal. At. Spectrom., 2023, **38**, 704–715 | **711**

Fig. 7 Histograms of Mo/Cu ratio distribution in single pixels of a kidney section taken from a rat given 60 mg per kg per day bischoline tetrathiomolybdate (TTM) imaged at 3×3 µm (a) and 20×18 µm pixel size (b). Data for low Mo concentration (<64 mg kg^{-1}) and high Mo concentration (>64 mg kg^{-1}) are shown separately.

patterns with the means of Mo/Cu equal to 0.90 and 0.76, correspondingly. In contrast, Mo/Cu distribution at 20 µm spot size does not show visible bimodality.

The mammalian kidney is one of the most complex organs in the body containing at least sixteen different highly specialized epithelial cell types. The number of specialized endothelial cells, immune cells, and interstitial cell types might be even larger.[61] The interplay between different cell types is critical for kidney function. Single-cell metallomics including high-resolution elemental imaging can complement single-cell techniques that involve transcriptomics, metabolomics, and proteomics, which provide new opportunities to classify cells in the kidney and understand their functions. Elemental imaging at the cellular to subcellular level can help to study, for example, the selective toxicity that can be seen following exposure to nephrotoxic substances, that is linked to the differences in response of the cells throughout the nephron of the kidney. Imaging at low-micrometre voxel size allows for determining metal concentrations not only in individual cells, but potentially at the level of organelles such as mitochondria that are typically 1–2 µm in length and contain 20–80% of the cell's iron, copper, and manganese imported for their redox activities,

primarily for electron transport.[62] Mitochondrial damages and dysfunction are recognized as a leading factor to many chronic and acute renal diseases[63] and an inorganic chemical insight into the state of the mitochondrial network would support the characterisation of nephrotoxic and aging effects by other methods.

Conclusions

A systematic approach towards quantitative bioimaging Mg, Cu, Zn, Mn and Fe in animal tissue using LA-ICP-TOFMS has been described in this paper for the first time. This involves the use of cryosectioned gelatin standards spiked with the elements of interest for calibration. Results from careful optimisation of instrumental parameters to achieve optimal limits of detection (in the low µg g^{-1} range) with a fit-for-purpose isotopic selectivity revealed that with ICP-TOFMS and a resolution power of approximately 6000 there is no need for gaining extra selectivity (e.g., by using collision/reaction gases) for the investigated elements in the biological matrix. The homogeneity of gelatin standards spiked with nitric acid solutions was found comparable with that of pH-neutral salt solution making the use of HNO$_3$-based standards preferable due to the ease of preparation and the lower blank contributions. The linear response obtained between the signal intensity of all investigated elements and the gelatin thickness under constant laser fluence and repetition rate suggested the use of gelatin cryosections of a single thickness as feasible calibrants for tissue samples sectioned at a range of thicknesses. Finally, the high-resolution quantitative imaging method developed in this paper was extended to include Mo and applied to obtain quantification of Mg, Mn, Fe, Cu, Zn and Mo in the medulla regions of rat kidney from rats administered with a de-coppering Mo-based drug used for treatment of Wilson's disease. The spatially resolved elemental data obtained at cellular and subcellular resolution, provided invaluable information on the relationship between drug-related and endogenous elements, e.g., through Mo/Cu ratio monitoring.

Author contributions

S. Strekopytov: conceptualization, methodology, investigation, formal analysis, validation, visualization, writing – original draft, writing – review & editing. K. Billimoria: conceptualization, methodology, investigation, writing – review & editing. H. Goenaga Infante: conceptualisation, methodology, resources, supervision, writing – review & editing, funding acquisition.

Conflicts of interest

There are no conflicts to declare.

Acknowledgements

712 | J. Anal. At. Spectrom., 2023, 38, 704–715

This journal is © The Royal Society of Chemistry 2023

Strategy (BEIS) through the UK National Measurement System Chemical and Biological Metrology Programme.

References

1 W. Maret, Metalloproteomics, metalloproteomes, and the annotation of metalloproteins, *Metallomics*, 2010, **2**, 117–125.

2 K. J. Barnham and A. I. Bush, Biological metals and metal-targeting compounds in major neurodegenerative diseases, *Chem. Soc. Rev.*, 2014, **43**, 6727–6749.

3 O. Bandmann O, K. H. Weiss and S. G. Kaler, Wilson's disease and other neurological copper disorders, *Lancet Neurol.*, 2015, **14**, 103–113.

4 A. Gupte and R. J. Mumper, Elevated copper and oxidative stress in cancer cells as a target for cancer treatment, *Cancer Treat. Rev.*, 2009, **35**, 32–46.

5 S. Rottenberg, C. Disler and P. Perego, The rediscovery of platinum-based cancer therapy, *Nat. Rev. Cancer*, 2021, **21**, 37–50.

6 T. Hanawa, Metal ion release from metal implants, *Mater. Sci. Eng., C*, 2004, **24**, 745–752.

7 A. Limbeck, P. Galler, M. Bonta, G. Bauer, W. Nischkauer and F. Vanhaecke, Recent advances in quantitative LA-ICP-MS analysis: challenges and solutions in the life sciences and environmental chemistry, *Anal. Bioanal. Chem.*, 2015, **407**, 6593–6617.

8 M. Martinez and M. Baudelet, Calibration strategies for elemental analysis of biological samples by LA-ICP-MS and LIBS – A review, *Anal. Bioanal. Chem.*, 2020, **412**, 27–36.

9 C. Arnaudguilhem, M. Larroque, O. Sgarbura, D. Michau, F. Quenet, S. Carrère, B. Bouyssière and S. Mounicou, Toward a comprehensive study for multielemental quantitative LA-ICP MS bioimaging in soft tissues, *Talanta*, 2021, **222**, 121537.

10 O. B. Bauer, O. Hachmöller, O. Borovinskaya, M. Sperling, H.-J. Schurek, G. Ciarimboli and U. Karst, LA-ICP-TOF-MS for rapid, all-elemental and quantitative bioimaging, isotopic analysis and the investigation of plasma processes, *J. Anal. At. Spectrom.*, 2019, **34**, 694–701.

11 M. Zoriy and J. S. Becker, Imaging of elements in thin cross sections of human brain samples by LA-ICP-MS: a study on reproducibility, *Int. J. Mass Spectrom.*, 2007, **264**, 175–180.

12 T. Van Acker, S. J. M. Van Malderen, L. Colina-Vegas, R. K. Ramachandran and F. Vanhaecke, Selective ablation of biological tissue and single cells on a glass substrate by controlling the laser energy density of nanosecond 193 nm laser radiation, *J. Anal. At. Spectrom.*, 2019, **34**, 1957–1964.

13 D. N. Douglas, A. J. Managh, H. J. Reid and B. L. Sharp, High-speed, integrated ablation cell and dual concentric injector plasma torch for laser ablation–inductively coupled plasma mass spectrometry, *Anal. Chem.*, 2015, **87**, 11285–11294.

14 Elemental Scientific Lasers, LLC, *Application Note: the TwoVol3 Ablation Cell for NWR Platform*, Bozeman, MT, 2020.

15 Teledyne Photon Machines, Inc., *Iridia: Engineered by Science [flyer]*, 2022.

16 S. J. M. Van Malderen, T. Van Acker and F. Vanhaecke, Sub-micrometer nanosecond LA-ICP-MS imaging at pixel acquisition rates above 250 Hz via a low-dispersion setup, *Anal. Chem.*, 2020, **92**, 5756–5764.

17 D. Bleiner, K. Hametner and D. Günther, Optimization of a laser ablation-inductively coupled plasma "time of flight" mass spectrometry system for short transient signal acquisition, *Fresenius. J. Anal. Chem.*, 2000, **368**, 37–44.

18 J. Feldmann, A. Kindness and P. Ek, Laser ablation of soft tissue using a cryogenically cooled ablation cell, *J. Anal. At. Spectrom.*, 2002, **17**, 813–818.

19 M. Burger, A. Gundlach-Graham, S. Allner, G. Schwarz, H. A. O. Wang, L. Gyr, S. Burgener, B. Hattendorf, D. Grolimund and D. Günther, High-speed, high-resolution, multielemental LA-ICP-TOFMS imaging: Part II. Critical evaluation of quantitative three-dimensional imaging of major, minor, and trace elements in geological samples, *Anal. Chem.*, 2015, **87**, 8259–8267.

20 M. Tanner and D. Günther, A new ICP-TOFMS. Measurement and readout of mass spectra with 30 μs time resolution, applied to in-torch LA-ICP-MS, *Anal. Bioanal. Chem.*, 2008, **391**, 1211–1220.

21 L. Hendriks, A. Gundlach-Graham, B. Hattendorf and D. Günther, Characterization of a new ICP-TOFMS instrument with continuous and discrete introduction of solutions, *J. Anal. At. Spectrom.*, 2017, **32**, 548–561.

22 M. Tanner, Y. Bussweiler and O. Borovinskaya, Laser ablation and inductively coupled plasma–time-of-flight mass spectrometry – a powerful combination for high-speed multielemental imaging on the micrometer scale, *Spectroscopy*, 2017, **32**(5), 14–20.

23 T. Narukawa and S. Willie, Dried deposits of biological tissues solubilized using formic acid for LA ICP-TOF-MS, *J. Anal. At. Spectrom.*, 2010, **25**, 1145–1148.

24 S. M. Monk and S. M. Lev, Toxicological applications of cryogenic laser ablation inductively coupled plasma time of flight mass spectrometry (CLA-ICP-TOF-MS), *J. Anal. At. Spectrom.*, 2013, **28**, 274–279.

25 C. J. Greenhalgh, O. M. Voloaca, P. Shaw, A. Donard, L. M. Cole, M. R. Clench, A. J. Managh and S. L. Haywood-Small, Needles in haystacks: using fast-response LA chambers and ICP-TOF-MS to identify asbestos fibres in malignant mesothelioma models, *J. Anal. At. Spectrom.*, 2020, **35**, 2231–2238.

26 A. Schoeberl, M. Gutmann, S. Theiner, M. Schaier, A. Schweikert, W. Berger and G. Koellensperger, Cisplatin uptake in macrophage subtypes at the single-cell level by LA-ICP-TOFMS imaging, *Anal. Chem.*, 2021, **93**, 16456–16465.

27 A. Schweikert, S. Theiner, D. Wernitznig, A. Schoeberl, M. Schaier, S. Neumayer, B. K. Keppler and G. Koellensperger, Micro-droplet-based calibration for quantitative elemental bioimaging by LA-ICPMS, *Anal. Bioanal. Chem.*, 2022, **414**, 485–495.

28 A. Schweikert, S. Theiner, M. Šala, P. Vician, W. Berger, B. K. Keppler and G. Koellensperger, Quantification in bioimaging by LA-ICPMS – evaluation of isotope dilution

This journal is © The Royal Society of Chemistry 2023

J. Anal. At. Spectrom., 2023, **38**, 704–715 | 713

and standard addition enabled by micro-droplets, *Anal. Chim. Acta*, 2022, **1223**, 340200.

29 O. M. Voloaca, M. R. Clench, G. Koellensperger, L. M. Cole, S. L. Haywood-Small and S. Theiner, Elemental mapping of human malignant mesothelioma tissue samples using high-speed LA-ICP-TOFMS imaging, *Anal. Chem.*, 2022, **94**, 2597–2606.

30 K. Billimoria, Y. A. Diaz Fernandez, E. Andresen, I. Sorzabal-Bellido, G. Huelga Suarez, C. Ortiz-de-Solórzano, U. Resch-Gengerc and H. Goenaga Infante, The potential of 3D bioprinting for preparation of nanoparticle-based calibration standards for LA-ICP-ToF-MS quantitative imaging, *Metallomics*, 2022, **14**, mfac088.

31 D. J. Bellis and R. Santamaria-Fernandez, Ink jet patterns as model samples for the development of LA-ICP-SFMS methodology for mapping of elemental distribution with reference to biological samples, *J. Anal. At. Spectrom.*, 2010, **25**, 957–963.

32 B. Jackson, S. Harper, L. Smith and J. Flinn, Elemental mapping and quantitative analysis of Cu, Zn, and Fe in rat brain sections by laser ablation ICP-MS, *Anal. Bioanal. Chem.*, 2006, **384**, 951–957.

33 H. J. Stärk and R. Wennrich, A new approach for calibration of laser ablation inductively coupled plasma mass spectrometry using thin layers of spiked agarose gels as references, *Anal. Bioanal. Chem.*, 2011, **399**, 2211–2217.

34 J. S. Becker, M. V. Zoriy, C. Pickhardt, N. Palomero-Gallagher and K. Zilles, Imaging of copper, zinc, and other elements in thin section of human brain samples (hippocampus) by laser ablation inductively coupled plasma mass spectrometry, *Anal. Chem.*, 2005, **77**, 3208–3216.

35 R. Niehaus, M. Sperling and U. Karst, Study on aerosol characteristics and fractionation effects of organic standard materials for bioimaging by means of LA-ICP-MS, *J. Anal. At. Spectrom.*, 2015, **30**, 2056–2065.

36 J. S. Becker, M. V. Zoriy, M. Dehnhardt, C. Pickhardt and K. Zilles, Copper, zinc, phosphorus and sulfur distribution in thin section of rat brain tissues measured by laser ablation inductively coupled plasma mass spectrometry: possibility for small-size tumor analysis, *J. Anal. At. Spectrom.*, 2005, **20**, 912–917.

37 J. Dobrowolska, M. Dehnhardt, A. Matusch, M. Zoriy, N. Palomero-Gallagher, P. Koscielniak, K. Zilles and J. S. Becker, Quantitative imaging of zinc, copper and lead in three distinct regions of the human brain by laser ablation inductively coupled plasma mass spectrometry, *Talanta*, 2008, **74**, 717–723.

38 K. Billimoria, D. N. Douglas, G. Huelga-Suarez, J. F. Collingwood and H. Goenaga-Infante, Investigating the effect of species-specific calibration on the quantitative imaging of iron at mg kg^{-1} and selenium at μg kg^{-1} in tissue using laser ablation with ICP-QQQ-MS, *J. Anal. At. Spectrom.*, 2021, **36**, 1047–1054.

39 M. Birka, K. S. Wentker, E. Lusmöller, B. Arheilger, C. A. Wehe, M. Sperling, R. Stadler and U. Karst, Diagnosis of nephrogenic systemic fibrosis by means of elemental bioimaging and speciation analysis, *Anal. Chem.*, 2015, **87**, 3321–3328.

40 O. Hachmöller, A. Zibert, H. Zischka, M. Sperling, S. Reinartz Groba, I. Grünewald, E. Wardelmann, H. H.-J. Schmidt and U. Karst, Spatial investigation of the elemental distribution in Wilson's disease liver after D-penicillamine treatment by LA-ICP-MS, *J. Trace Elem. Med. Biol.*, 2017, **44**, 26–31.

41 M. Cruz-Alonso, B. Fernandez, A. Navarro, S. Junceda, A. Astudillo and R. Pereiro, Laser ablation ICP-MS for simultaneous quantitative imaging of iron and ferroportin in hippocampus of human brain tissues with Alzheimer's disease, *Talanta*, 2019, **197**, 413–421.

42 J. Liu, L. Zheng, X. Wei, B. Wang, H. Chen, M. Chen, M. Wang, W. Feng and J. Wang, Quantitative imaging of trace elements in brain sections of Alzheimer's disease mice with laser ablation inductively coupled plasma-mass spectrometry, *Microchem. J.*, 2022, **172**, 106912.

43 K. Kysenius, B. Paul, J. B. Hilton, J. R. Liddell, D. J. Hare and P. J. Crouch, A versatile quantitative microdroplet elemental imaging method optimised for integration in biochemical workflows for low-volume samples, *Anal. Bioanal. Chem.*, 2019, **411**, 603–616.

44 T. Van Helden, S. Braeuer, T. Van Acker, O. Leroux, D. Van Der Straeten and F. Vanhaecke, High-speed mapping of Hg and Se in biological tissue *via* laser ablation-inductively coupled plasma-mass spectrometry, *J. Anal. At. Spectrom.*, 2022, **37**, 1455–1461.

45 S. J. Van Malderen, E. Vergucht, M. De Rijcke, C. Janssen, L. Vincze and F. Vanhaecke, Quantitative determination and subcellular imaging of Cu in single cells via laser ablation-ICP-mass spectrometry using high-density microarray gelatin standards, *Anal. Chem.*, 2016, **88**, 5783–5789.

46 J. R. Foster, K. Billimoria, M. E. Del Castillo Busto, S. Strekopytov, H. Goenaga-Infante and T. J. Morley, Accumulation of molybdenum in major organs following repeated oral administration of bis-choline tetrathiomolybdate in the Sprague Dawley rat, *J. Appl. Toxicol.*, 2022, **42**, 1807–1821.

47 K. B. Billimoria, PhD Thesis, University of Warwick, 2022.

48 H. Timonen, M. Cubison, M. Aurela, D. Brus, H. Lihavainen, R. Hillamo, M. Canagaratna, B. Nekat, R. Weller, D. Worsnop and S. Saarikoski, Applications and limitations of constrained high-resolution peak fitting on low resolving power mass spectra from the ToF-ACSM, *Atmos. Meas. Tech.*, 2016, **9**, 3263–3281.

49 M. Burger, L. Hendriks, J. Kaeslin, A. Gundlach-Graham, B. Hattendorf and D. Günther, Characterization of inductively coupled plasma time-of-flight mass spectrometry in combination with collision/reaction cell technology – insights from highly time-resolved measurements, *J. Anal. At. Spectrom.*, 2019, **34**, 135–146.

50 J. Meija, T. Coplen, M. Berglund, W. Brand, P. De Bièvre, M. Gröning, N. Holden, J. Irrgeher, R. Loss, T. Walczyk and T. Prohaska, Isotopic compositions of the elements 2013 (IUPAC Technical Report), *Pure Appl. Chem.*, 2016, **88**, 293–306.

714 | *J. Anal. At. Spectrom.*, 2023, **38**, 704–715

This journal is © The Royal Society of Chemistry 2023

51 M. Burger, G. Schwarz, A. Gundlach-Graham, D. Käser, B. Hattendorf and D. Günther, Capabilities of laser ablation inductively coupled plasma time-of-flight mass spectrometry, *J. Anal. At. Spectrom.*, 2017, **32**, 1946–1959.

52 S. Bürger and L. R. Riciputi, A rapid isotope ratio analysis protocol for nuclear solid materials using nano-second laser-ablation time-of-flight ICP-MS, *J. Environ. Radioact.*, 2009, **100**, 970–976.

53 A. Gundlach-Graham, L. Hendriks, K. Mehrabi and D. Günther, Monte Carlo simulation of low-count signals in time-of-flight mass spectrometry and its application to single-particle detection, *Anal. Chem.*, 2018, **90**, 11847–11855.

54 M. Tanner, Shorter signals for improved signal to noise ratio, the influence of Poisson distribution, *J. Anal. At. Spectrom.*, 2010, **25**, 405–407.

55 M. T. Westerhausen, T. E. Lockwood, R. Gonzalez de Vega, A. Röhnelt, D. P. Bishop, N. Cole, P. A. Doble and D. Clases, Low background mould-prepared gelatine standards for reproducible quantification in elemental bio-imaging, *Analyst*, 2019, **144**, 6881–6888.

56 C. Austin, F. Fryer, J. Lear, D. Bishop, D. Hare, T. Rawling, L. Kirkup, A. McDonagh and P. Doble, Factors affecting internal standard selection for quantitative elemental bio-imaging of soft tissues by LA-ICP-MS, *J. Anal. At. Spectrom.*, 2011, **26**, 1494–1501.

57 J. A. T. Pugh, A. G. Cox, C. W. McLeod, J. Bunch, B. Whitby, B. Gordon, T. Kalber and E. White, A novel calibration strategy for analysis and imaging of biological thin sections by laser ablation inductively coupled plasma mass spectrometry, *J. Anal. At. Spectrom.*, 2011, **26**, 1667–1673.

58 B. K. Maiti and J. J. Moura, Diverse biological roles of the tetrathiomolybdate anion, *Coord. Chem. Rev.*, 2021, **429**, 213635.

59 R. F. Reinoso, B. A. Telfer and M. Rowland, Tissue water content in rats measured by desiccation, *J. Pharmacol. Toxicol. Methods*, 1997, **38**, 87–92.

60 G. J. Brewer, R. D. Dick, V. Yuzbasiyan-Gurkan, R. Tankanow, A. B. Young and K. J. Kluin, Initial therapy of Wilson's disease patients with tetrathiomolybdate, *Arch. Neurol.*, 1991, **48**, 42–47.

61 M. S. Balzer, T. Rohacs and K. Susztak, How many cell types are in the kidney and what do they do?, *Annu. Rev. Physiol.*, 2022, **84**, 507–531.

62 F. Thévenod, W.-K. Lee and M. D. Garrick, Iron and cadmium entry into renal mitochondria: physiological and toxicological implications, *Front. Cell Dev. Biol.*, 2020, **8**, 848.

63 P. Duann and P.-H. Lin, Mitochondria damage and kidney disease, in *Mitochondrial Dynamics in Cardiovascular Medicine*, ed. G. Santulli, Springer, Cham, Switzerland, 2017, pp. 529–551.

This journal is © The Royal Society of Chemistry 2023

J. Anal. At. Spectrom., 2023, **38**, 704–715 | **715**